HHS Public Access

Author manuscript

J Magn Reson Imaging. Author manuscript; available in PMC 2018 May 15.

Published in final edited form as:

J Magn Reson Imaging. 2015 September ; 42(3): 698–708. doi:10.1002/jmri.24819.

2D phase sensitive inversion recovery imaging to measure in-vivo spinal cord gray and white matter areas in clinically feasible acquisition times

N. Papinutto, PhD[1,*], **R. Schlaeger, MD**[1,2], **V. Panara, MD**[3], **E. Caverzasi, MD**[1], **S. Ahn, PhD**[4], **K.J. Johnson, BA, RT**[4], **A.H. Zhu, MS**[1], **W.A. Stern, RT**[1], **G. Laub, PhD**[4], **S.L. Hauser, MD**[1], and **R.G. Henry, PhD**[1,5,6]

[1]Department of Neurology, University of California San Francisco, San Francisco, CA, United States [2]Department of Neurology, University of Basel, Basel, Switzerland [3]ITAB - Institute of Advanced Biomedical Technologies, University "G. D'Annunzio", Chieti, Italy [4]Siemens Healthcare USA, San Francisco, CA, United States [5]Bioengineering Graduate Group, University of California San Francisco, San Francisco and University of California Berkeley, Berkeley, California, USA [6]Department of Radiology and Biomedical Imaging, University of California San Francisco, San Francisco, California, USA

Abstract

PURPOSE—In-vivo assessment of spinal cord gray matter (GM) and white matter (WM) could become pivotal to study various neurological diseases, but it is challenging because of insufficient GM/WM contrast provided by conventional MRI. Here we present and assess a procedure for measurement of spinal cord total cross-sectional area (TCA) and GM areas based on phase sensitive inversion recovery imaging (PSIR).

MATERIALS AND METHODS—We acquired 2D PSIR images at 3T at each disc level of the spinal axis on 10 healthy subjects and measured TCA, cord diameters, WM and GM area, and GM area/TCA ratio. We secondly investigated 32 healthy subjects at 4 selected levels (C2–C3, C3–C4, T8–T9, T9–T10, total acquisition time <8 minutes) and generated normative reference values of TCA and GM areas. We assessed test-retest, intra- and inter-operator reliability of the acquisition strategy and measurement steps.

RESULTS—The measurement procedure based on 2D PSIR imaging allowed TCA and GM area assessments along the entire spinal cord axis. The tests we performed revealed high test-retest/intra-operator reliability (mean coefficient of variation (COV) at C2–C3: TCA=0.41%, GM area=2.75%) and inter-operator reliability of the measurements (mean COV on the 4 levels: TCA=0.44%, GM area= 4.20%; mean intra-class correlation coefficient: TCA=0.998, GM area=0.906).

[*]Corresponding author: Nico Papinutto, PhD, University of California, San Francisco, Dept. of Neurology, Tel: 415-502-7253, Fax: 415-353-9423, nico.papinutto@ucsf.edu.

Conflict of interest

S.L.H. currently serves on the scientific advisory boards of Symbiotix and Bionure.

CONCLUSION—2D PSIR allows reliable in-vivo assessment of spinal cord TCA, GM and WM areas in clinically feasible acquisition times. The area measurements presented here are in agreement with previous MRI and post-mortem studies.

Keywords

Spinal cord; magnetic resonance imaging; anatomy; morphometry; gray matter; white matter

INTRODUCTION

During the last two decades MRI of the human spinal cord has gained a fundamental role in the diagnosis and monitoring of various diseases including traumatic injuries, spondylotic myelopathy, vascular pathologies, tumors and inflammatory diseases such as neuromyelitis optica (NMO) and multiple sclerosis (MS) (1,2).

Progressive disability in MS is thought to be driven by spinal cord involvement that may affect both the gray matter (GM) and white matter (WM) compartments (3,4).

Demyelination, axonal and neuronal loss, and metabolic changes that may lead to disability in MS patients have been studied in-vivo in the spinal cord using several quantitative MR techniques (5–16). However, the widespread clinical application of these promising MR techniques is still challenging due to the small dimension of the cord, susceptibility effects, and subject and physiological motion artifacts related to heartbeat and breathing (17). Therefore, with regard to MS and other cord specific pathologies, conventional anatomical imaging remains by far the most widely used tool.

GM and WM compartment-specific morphometry of the spinal cord was precisely described in an autopsy series by Kameyama and coauthors (18), based on 12 spinal cords without evidence of any nervous system disease. Their study provided anatomic descriptions and morphometric assessments at each spinal segment, including measurements of total cross-sectional areas (TCA), GM and WM areas, and transverse and sagittal diameters. However, earlier studies on brain autopsies suggested that the volumes of WM and GM compartments are influenced to a different extent by the fixation process (19). Therefore, the reported ex-vivo morphometric assessments and proportions of the spinal cord GM and WM compartments may not agree with in-vivo values.

Anatomical spinal cord imaging might greatly profit from a method that allows precise in-vivo morphometric and compartment-specific assessments of the entire spinal cord axis. Conventional contrast-based anatomical MR techniques, though still commonly used for MS and other spinal cord pathologies, provide limited spinal cord detail. Poor contrast between GM and WM from conventional clinical T1 or T2 weighted MRI and artifacts common to all spinal cord imaging modalities have impeded in-vivo assessment of the spinal cord GM and WM compartments, especially in the thoracic levels (20). T2 weighted MRI in healthy controls has mostly focused on TCA measurements of the entire spinal cord axis (21) or cervical cord only (22,23). Recently, 3D gradient echo (GRE) (14,24) or 2D multi-echo GRE-based sequences have been used for in-vivo compartment-specific assessments and for atlas constructions, as their T2* weighting provides a good GM/WM contrast (25–28).

However, since the quality of T2* images is not always consistent, this modality is still not routinely and clinically used for precise in-vivo morphometric and compartment-specific assessments of the entire spinal axis.

Since the first MRI experiments, it has been known that the (T1 weighted) image contrast and signal to noise ratios can be enhanced by doubling the dynamic range of the longitudinal magnetization (i.e. including both positive and negative values) by preserving the sign of the MR signal intensity in an inversion recovery sequence with a real reconstruction (29,30). An accurate real reconstruction of inversion recovery images, however, requires correction of phase errors artifacts that arise when restoring the magnetization polarity, and it's referred to as phase sensitive inversion recovery (PSIR) imaging.

Different phase-correction strategies have been investigated in the past 30 years, including the acquisition of additional reference images, multiple IR acquisitions and the estimation of phase from local statistics using various phase correction algorithms (31–35).

The most commonly applied method in PSIR imaging achieves the magnetization polarity restoration by interleaving a reference scan into the regular image acquisition scans (32,36). Using this reference, phase variations caused by the system (the background phase modulation) are identified and removed from the original acquisition, allowing a correct restoration of the magnetization polarity.

PSIR imaging has been used in the brain (37), in particular to monitor the progress of myelination and brain maturation (38), and to explore the myelinization of cortical areas (39). The enhanced contrast offered by PSIR has also been found useful for improving the identification of deep gray matter structures such as the subthalamic nucleus and globus pallidus (40,41).

In the last few years, PSIR imaging gained increased interest regarding the detection of cortical lesions in MS, as PSIR imaging was shown to have a complementary or even alternative value to DIR (double inversion recovery) imaging, which is currently considered the standard sequence for cortical lesion detection (42–44).

Recently two pilot-studies applied the 3D PSIR technique to the cervical spinal cord (45,46) of MS patients and demonstrated a very good contrast between spinal cord GM/WM and WM/CSF. One further study reported a high efficiency in MS lesion detection using sagittal PSIR (47) in the cervical cord.

In this cross-sectional study we used 2D PSIR to quantitatively assess spinal cord TCA, WM and GM areas with three-fold goals:

- To assess the efficiency of the proposed acquisition and measurement procedure along the entire spinal cord axis with reference to the in-vivo studies based on T2* contrast and the anatomical post-mortem data by Kameyama and coauthors (18).
- To provide normative values of TCA, GM areas, GM area/TCA ratio and cord diameters at selected levels of the spinal cord representative of the upper cervical

and lower thoracic portions, that could be routinely acquired in a clinically acceptable acquisition time of less than 2 minutes per level.

- To assess the scan-rescan, intra- and inter-operator reproducibility of the TCA and GM measurements of the procedure presented in this study.

MATERIALS AND METHODS

MR Imaging

Thirty-two healthy subjects (14 men: mean±std (standard deviation) age 46.8±13.4; 18 women: mean±std age 50.4±15.1; total cohort: age 28–78; mean±std 48.8±14.3) underwent MRI scanning on a 3T whole body system (Skyra, Siemens Medical Solutions, Erlangen, Germany) equipped with a 20-channel head/neck coil and a 32-channel spine coil. To minimize neck movement during the examination, each subject was provided with an MR compatible cervical collar (14).

Research was performed in compliance with the Code of Ethics of the World Medical Association (Declaration of Helsinki), and the Committee on Human Research of our Institution approved the study protocol. All subjects provided written informed consent to participate in this study. None of the subjects had any history of psychiatric, neurological or cognitive impairment.

2D PSIR imaging (pulse sequence diagram reported in Fig. 1) was performed on each participant with the following parameters: 0.78*0.78 mm^2 axial in-plane resolution, 5 mm slice thickness, 256×256 matrix size, TR/TE/TI=4000/3.22/400 ms, flip angle=10°, and 3 averages (acquisition time: 1:50 min per level). Two images were created by the scanner for each acquisition: one with a magnitude reconstruction and the other with a phase-sensitive reconstruction. The resolution of images, which is slightly lower than the resolution used in previous work based on T2* imaging was chosen to minimize the acquisition time and make the procedure feasible in a clinical setting, whenever the selection of particular levels of the spinal cord can help in answering to specific clinical questions. Standard T2-weighted sagittal images of the cervical and thoracic portions of the cord were also acquired and used for the correct positioning of the 2D PSIR acquisitions.

For in-vivo quantification, precise anatomical description of the GM and WM compartments along the entire spinal cord axis and their comparison to post-mortem data (18) and other reported MRI data, we first focused the assessments on 10 younger subjects with a homogenous gender and age distribution (5 men and 5 women, mean age±std 37.7±7.5 years). In this group PSIR acquisitions were repeated at all disc spaces along the entire spinal cord axis from C1–C2 down to the medullary conus (T12-L1) using the vertebral disc as reference and positioning the slices perpendicular to the spinal cord. Secondly, we extended the sample to 32 participants, but restricted the acquisition and analysis to 4 representative vertebral disc levels (C2–C3, C3–C4, T8–T9 and T9–T10) that could be routinely acquired in a clinical environment in less than 8 minutes. C2–C3 is the standard level explored in MS studies (46,48–52), while the C3–C4 and the selected thoracic levels, just above the lumbar enlargement, were less explored in this regard. T8–T9 and T9–T10

were chosen since we hypothesized that the GM and total cord areas at these levels might be potential markers of spinal cord function regarding the lower limbs.

Area And Metric Measurements

Total spinal cord and GM areas at the different levels were calculated on the phase-sensitive reconstructed images using the software Jim (Version 6.0, Xinapse Systems, Northants, United Kingdom; www.xinapse.com). The total cross-sectional area was estimated in a semi-automated way (53); briefly this was done using the cord finder toolkit with fixed settings (nominal cord diameter 8mm, number of shape coefficients 24, order of longitudinal variation 12). The marker requested by the toolkit was positioned on the mid-sagittal WM, directly posterior to the gray commissure.

A neuroradiologist with 5 years of experience (VP) manually segmented the GM area three times using Jim. The average GM area was calculated. The spinal cord WM area was calculated as the difference between the TCA and the average GM area. An example of the acquisition prescription and TCA and GM segmentation of a representative subject are shown in Fig. 2. Two orthogonal lengths of the cord were measured with Jim using the boundary of the total cord delineated with the semi-automatic method as a reference: the sagittal diameter was defined as the measure of the ROI in the mid-sagittal line, while the transverse diameter was defined as the largest dimension of the cord perpendicularly to the mid-sagittal line.

Evaluation Of Reproducibility And Contrast To Noise Ratio

A series of experiments was performed to evaluate the reproducibility and precision of the area measurements and the contrast to noise ratio (CNR) of images as follows.

Experiment A)—Scan-rescan intra- and inter-operator reproducibility of the TCA and GM area measurements were evaluated. Four separate scans were performed on a single healthy subject at the C2–C3 and C3–C4 level with full repositioning between scans. The TCA of the cord at these levels was measured by 3 different operators (NP, MRI physicist with 10 years of experience in neuroimaging, VP, neuroradiologist with 5 years of experience and RS, neurologist with 10 years of experience) using the software Jim semi-automatically on the 4 separate acquisitions. GM areas were measured at these levels by 2 experienced operators (VP, RS). Intra-operator reproducibility was assessed by calculating the coefficient of variation (COV = standard deviation/mean of the values) across the 4 scan-rescan samples per operator. Inter-operator reproducibility was assessed using the COV across operators on each of the 4 acquisitions; these four coefficients were then averaged.

Experiment B)—For 8 healthy subjects (25% of the whole cohort) the cord TCAs were independently measured at the C2–C3, C3–C4, T8–T9, T9–T10 levels by 3 operators (NP, VP and RS) to provide inter-operator reliability for cervical and thoracic cord levels. GM areas at the 4 disc levels of these subjects were independently measured by VP and RS. Inter-operator reliability of the measurements was calculated as COV and as single measures intra-class correlation coefficients (ICC).

Experiment C)—For 10 healthy subjects the CNR for CSF/WM and for WM/GM tissues was calculated on the images acquired at the C2–C3 level.

CNR between tissue 1 and tissue 2 was defined as $CNR_{12}=|S_1-S_2|/BN$, where S_1 and S_2 were the average signals in two identical 2×2 voxels square ROIs positioned on the tissues and BN was the standard deviation of the signal measured in a ROI of 100 mm^2 area outside the neck, away from imaging artifacts (background noise [BN]).

The GM ROI was positioned on the anterior horn, the WM ROI on the lateral column.

Statistical Analysis

Statistical analysis was performed using IBM SPSS Statistics (Version 21, 2012, IBM Corp.) and JMP Statistics (www.jmp.com, Version 11, 2013, SAS Institute). In the full cohort of 32 controls, the values of TCA, GM, WM area and GM area/TCA at all the 4 levels were assessed for normality of the distribution of data using the Shapiro-Wilk W tests.

Correlations of TCA and GM areas among the four levels were investigated by calculating Pearson product-moment correlation coefficients.

RESULTS

Evaluation Of Reproducibility And Contrast To Noise Ratio

Experiment A)

Intra- And Inter-Operator Reproducibility Of Cord Area Measurements From Scan-Rescan Acquisitions (Table 1): For the 4 test-retest acquisitions at the C2–C3 level, TCA intra-operator reproducibility COVs for the 3 operators were 0.40%, 0.51% and 0.32% (mean: 0.41%). GM area intra-operator reproducibility COVs for the 2 operators were 2.17% and 3.33% (mean: 2.75%). The average of inter-operator COV for the different operators across the 4 acquisitions was 0.25% for TCA, and 0.90% for GM areas. At the C3–C4 level TCA intra-operator reproducibility COVs for the 3 operators were 1.86%, 1.85% and 2.62% (mean: 2.11%). GM area intra-operator reproducibility COVs for the 2 operators were 2.40% and 2.71% (mean: 2.55%). The average of inter-operator COV for the different operators across the 4 acquisitions was 0.40% for TCA, and 2.60% for GM area. The higher intra- compared to inter-operator variability suggests that the difference of semi-automatic segmentation across operators for the area measurement is contributing less to the overall test-retest reproducibility than the variability from the repositioning of the subject in the scanner and the positioning of the acquired slice.

Experiment B)

Inter-Operator Reliability (Table 2): On the 8 subjects the inter-operator COVs for the TCA at C2–C3, C3–C4, T8–T9 and T9–T10 levels were 0.35%, 0.25%, 0.43% and 0.71%, respectively (mean on the levels: 0.44%). The single measures ICCs at the 4 levels for TCA were 0.999, 0.998, 0.996 and 0.998, respectively (mean on the levels: 0.998). For the GM area on the 8 subjects the values of inter-operator COVs at the 4 levels were 3.18%, 3.99%,

5.90% and 3.72% (mean on the levels: 4.20%), and the single measures ICCs were 0.916, 0.888, 0.908 and 0.912, respectively (mean on the levels: 0.906).

Experiment C)—The average CNR for 10 subjects (mean±std) was 44.52±13.74 for CSF/WM and 15.19±5.09 for WM/GM.

Area And Metric Measurements

In all 32 subjects images obtained at the 4 spinal cord levels were evaluated by NP (MRI physicist with 10 years of experience in neuroimaging), VP (neuroradiologist with 5 years of experience) and RS (neurologist with 10 years of experience) and judged as having a good GM/WM contrast. For 2 subjects who underwent image acquisition at the beginning of the study the 2 thoracic levels were not acquired. In the subgroup of 10 subjects on which the entire spinal cord axis was acquired, the quality of the images was assessed by VP and RS and was found to be good at the cervical levels and the lower thoracic/lumbar levels, while at the mid thoracic levels (indicatively from T1–T2 to T7–T8) the quality was found to be sometimes suboptimal. However, it was sufficient for a GM delineation and TCA calculation.

As a demonstration of the technique Fig. 3 shows the PSIR images acquired at 6 levels along the entire spinal cord axis in a representative single subject.

The shape of the GM structure differed along the cord as reported in post-mortem anatomic descriptions (18). GM was approximately “M” shaped in the top cervical and central thoracic levels, “π” shaped in the lower cervical and upper thoracic levels and “X” shaped at the lumbar levels just above the conus.

Cord measures are summarized in Table 3 where spinal cord levels acquired for all 32 subjects are shown in gray while other lines only refer to the 10 subjects whose entire spinal cord axis was imaged. At the 4 selected levels TCA, WM, GM area, and the GM area/TCA ratio were normally distributed on the entire cohort, with the only exception of GM area at the T8–T9 level.

From the measurements of the TCA and GM areas along the entire spinal cord axis, 2 maxima in TCA and GM area were consistently determined (Fig. 4): the first one at the disc level C4–C5 and the second one in a slightly more variable region centered at the T11–T12 disc level. These two maxima of the TCA and GM area represent the cervical and lumbar enlargements of the spinal cord and they are caused by increased neural input and output to the upper and lower limbs, respectively. The two enlargements are separated from T1–T2 to T9–T10 by a plateau (Fig. 4a and 4b). A relatively stable GM area/TCA ratio for most of the cervical and thoracic cord levels and a remarkable increase at the lower thoracic levels suggest a main contribution of GM to the lumbar enlargement, reflecting the decreasing number of ascending and descending WM tracts at the more caudal portions of the cord (Fig. 4e).

Similarly to the results of the TCA and the GM areas, the transverse diameter showed an absolute maximum at the disc level C4–C5 and a second smaller peak around T11–T12 (Fig.

4c). The sagittal diameter was found to be approximately constant across the cord, with two relatively small local maxima at C1–C2 and at T11–T12 (Fig. 4d). The ratio between the two diameters was highest around C4–C5, where the transverse diameter was about double than the sagittal diameter. In the thoracic spine down to the lower levels, instead, the shape of the cord was more rounded, with the transverse diameter remarkably diminishing if compared with the cervical levels, and the sagittal diameter almost constant (Fig. 4f). The transverse diameter was found to have slightly less variability across subjects compared to the sagittal diameter (see Fig. 4 and standard deviations/mean values in Table 3).

TCAs normalized to the T8–T9 and C2–C3 TCA values (g and h respectively) for each subject are shown at the bottom of Fig. 4. These in-vivo results are in agreement with the effects of normalization described by Kameyama et al. (18). Values normalized to C2–C3 are also reported in the last column of Table 3.

Average group results for TCA, GM and WM areas across the entire spinal cord axis are shown in Fig. 5. Like in Table 3, the data reported here are based on 32 subjects at the C2–C3, C3–C4, T8–T9 and T9–T10 disc levels and on 10 subjects at all other levels.

Cord Measures Associations Within The Cord

The associations among TCA and GM area values at the 4 different levels (C2–C3, C3–C4, T8–T9, T9–T10) are reported in Table 4. Since this was an explorative and qualitative analysis, no correction for multiple comparison was performed.

DISCUSSION

The goals of this cross-sectional study were three-fold. First we wanted to assess if the in-vivo MR acquisition and measurement procedure based on 2D phase-sensitive inversion recovery imaging that we present allows in-vivo quantification and anatomical description of the GM and WM compartments at each disc level along the entire spinal cord axis. In the 10 subjects we were able to acquire good quality images at all levels of the spinal cord. The GM/WM and WM/CSF contrasts was generally good and sufficient to segment and measure TCA, GM area and cord diameters, at each of the acquired levels from disc level C1–C2 down to the medullary conus (T12-L1), in each subject. By comparing results with a previous post-mortem study (18) we showed that our procedure enables accurate morphological and quantitative exploration of the entire spinal cord axis. Results obtained with the 2D PSIR imaging technique were in agreement with the findings previously reported in the few in-vivo MRI studies based on T2* acquisition techniques (14,24–28).

Second, we applied this method to explore 4 selected cord levels in an extended cohort of 32 healthy subjects, providing a set of normative values of the different metrics obtainable with the 2D PSIR. The quality of images at the 4 levels allowed TCA and GM area measurements with high test-retest, intra-operator and inter-operator reliability. In particular at the C2–C3 and T9–T10 levels, the quality of images, COV and ICC were particularly good, suggesting that these two levels are the best candidates to represent the cervical and low thoracic portion of the spinal cord in a clinically feasible acquisition time of less than 4 minutes.

The TCA values and diameters of the spinal cord that we measured are larger than the values reported by Kato and coauthors (23) by using T2 weighted images. As only few details of the measurements and methods were provided in that paper it is difficult to perform a fair comparison. However, in general, one can assume that the differences might be due to a different definition of the cord boundary on images with different contrast and resolution, or maybe, to effects inherent to the different populations under investigation. Our results of GM area, TCA, GM area/TCA, diameters are instead very similar to the data reported in studies based on a T2* acquisition (see for example Table 4 in Ref. (24), Fig. 6 in Ref. (25), and Fig. 4 in Ref. (28)). However, while the scan-rescan, intra- and inter-operator reproducibility of TCA measurements obtained with the presented procedure were very similar to the ones reported with the T2* based acquisitions (14), the scan-rescan, intra- and inter-operator reproducibility of GM area measurements we obtained in the present study were higher (14,25,28). This suggests that the 2D PSIR based protocol might be a reliable alternative to the methods used so far to assess in-vivo spinal cord compartments.

Our results are in agreement with the general morphometric relationships reported in Table 1, Fig. 1 and Fig. 2 of the post-mortem study by Kameyama et al. (18) for all the measured quantities (TCA, diameters, GM areas). It is important to emphasize that our cord level definition refers to the vertebral space, while in the post mortem study levels were defined according to the segmental level. We were able to delineate the curves of TCA, WM and GM area in vivo along the spinal cord down to the medullary conus. These curves are generally characterized by two maxima representing the cervical and lumbar enlargements (areas of increased neural input and output to the upper and lower limbs, respectively). The relative increase of the GM/cord area ratios at the lower thoracic levels with otherwise relatively stable GM/cord area ratios suggests a main contribution of GM to the lumbar enlargement, reflecting the decreasing number of ascending and descending WM tracts at the more caudal portions of the cord. In agreement with the post-mortem measurements by Kameyama and coauthors, the GM/cord area ratio at the cervical enlargement did not substantially increase in comparison with the more rostral levels. This finding is indicative of a concomitant contribution of both WM and GM to the cervical enlargement.

In agreement with previous reports based on T2* weighted imaging (24,25,28), the in-vivo TCAs in this study exceeded the corresponding post-mortem measurements by Kamayama and coauthors by about 30–35%, GM areas even by 50–60% at some cord levels. These findings suggest that the fixation-related shrinkage affects spinal cord WM and GM in different ways, as was already described in brain tissues by Kretschmann and coauthors (19). Therefore inferences on compartment-specific cord atrophy based on post-mortem studies have to be made with caution.

Kameyama and coauthors (18) expressed the idea that “any segment in an individual is calculable from measurement of a single normal segment”, and they tested it in particular with reference to C2–C3. Our data support this statement: TCA and GM area values showed strong correlations among the 4 measured levels. Moreover, normalization of TCA to the C2–C3 level had markedly reduced variability. The normalization to the C2–C3 level, for example, reduced the %RSD (ratios of the group standard deviation and the respective means) at all levels (20% average reduction from C1–2 to T10–11).

The strong correlations between adjacent cervical and adjacent thoracic levels further suggests that a selection of just the C2–C3 and T9–T10 levels (where measurements showed the highest precision), might be the most informative and efficient with a total acquisition time of less than 4 minutes.

Limitations of the current study include the relatively small number of subjects that underwent the entire spinal cord axis protocol, as this part of the study was intended to be explorative. Based on the entire spinal cord axis observations we selected 4 levels, in order to enhance applicability in larger cohorts and examined these levels in a larger cohort. A further major limitation of the study is that GM area was segmented manually, as a fully automated method is not yet available. All the tools we tested require substantial manual corrections and careful supervision of results by the operator (14). We therefore decided to test the fully manual method with ROIs delineated by neuroradiology experts. As both the inter- and intra-operator reliabilities were high, the GM areas in the larger cohort were delineated by a single operator.

Finally, since the method was tested in-vivo and not on a true reference standard with known values, its accuracy has to be further investigated.

In conclusion, we present a novel MRI quantitative procedure based on a 2D phase-sensitive inversion recovery imaging, which allows in-vivo characterization of the spinal cord GM and WM compartments at selected levels with high precision and reliablity and in clinically feasible acqusition times. We suggest that 2D PSIR imaging could be routinely used to explore cervical and thoracic selected levels in less than 2 minutes per level. The values obtained in this study from healthy controls might be applicable to future disease and healthy controls studies. Distinct assessments of GM and WM compartments may be pivotal for the understanding of the pathological mechanism leading to cord atrophy in various neurological diseases.

Acknowledgments

The authors acknowledge Refujia Gomez, Caroline Ciocca, Rachel Kanner and Alan Evangelista for help with data acquisition and/or data management. R.S. was funded by the Swiss MS Society and the Gottfried and Julia Bangerter-Rhyner Foundation, Switzerland. This research was supported by the National Institutes of Health (R01 NS049477; 1U19A1067152), and the National Multiple Sclerosis Society (RG 2899-D11).

References

1. Do-Dai DD, Brooks MK, Goldkamp A, Erbay S, Bhadelia RA. Magnetic resonance imaging of intramedullary spinal cord lesions: a pictorial review. Curr Probl Diagn Radiol. 2010; 39(4):160–185. [PubMed: 20510754]
2. Wheeler-Kingshott CA, Stroman PW, Schwab JM, et al. The current state-of-the-art of spinal cord imaging: Applications. NeuroImage. 2014; 84:1082–1093. [PubMed: 23859923]
3. Gilmore CP, DeLuca GC, Bo L, et al. Spinal cord neuronal pathology in multiple sclerosis. Brain Pathol. 2009; 19(4):642–649. [PubMed: 19170682]
4. Schlaeger R, Papinutto N, Panara V, et al. Spinal cord gray matter atrophy correlates with multiple sclerosis disability. Ann Neurol. 2014
5. Valsasina P, Rocca MA, Agosta F, et al. Mean diffusivity and fractional anisotropy histogram analysis of the cervical cord in MS patients. NeuroImage. 2005; 26(3):822–828. [PubMed: 15955492]

6. Agosta F, Absinta M, Sormani MP, et al. In vivo assessment of cervical cord damage in MS patients: a longitudinal diffusion tensor MRI study. Brain. 2007; 130(Pt 8):2211–2219. [PubMed: 17535835]
7. Wheeler-Kingshott CA, Hickman SJ, Parker GJ, et al. Investigating cervical spinal cord structure using axial diffusion tensor imaging. NeuroImage. 2002; 16(1):93–102. [PubMed: 11969321]
8. Freund P, Wheeler-Kingshott C, Jackson J, Miller D, Thompson A, Ciccarelli O. Recovery after spinal cord relapse in multiple sclerosis is predicted by radial diffusivity. Mult Scler. 2010; 16(10): 1193–1202. [PubMed: 20685759]
9. van Hecke W, Nagels G, Emonds G, et al. A diffusion tensor imaging group study of the spinal cord in multiple sclerosis patients with and without T2 spinal cord lesions. J Magn Reson Imaging. 2009; 30(1):25–34. [PubMed: 19557843]
10. Kearney H, Schneider T, Yiannakas MC, et al. Spinal cord grey matter abnormalities are associated with secondary progression and physical disability in multiple sclerosis. J Neurol Neurosurg Psychiatry. 2014
11. Kendi AT, Tan FU, Kendi M, Yilmaz S, Huvaj S, Tellioglu S. MR spectroscopy of cervical spinal cord in patients with multiple sclerosis. Neuroradiology. 2004; 46(9):764–769. [PubMed: 15258708]
12. Bjartmar C, Kidd G, Mork S, Rudick R, Trapp BD. Neurological disability correlates with spinal cord axonal loss and reduced N-acetyl aspartate in chronic multiple sclerosis patients. Ann Neurol. 2000; 48(6):893–901. [PubMed: 11117546]
13. Ciccarelli O, Wheeler-Kingshott CA, McLean MA, et al. Spinal cord spectroscopy and diffusion-based tractography to assess acute disability in multiple sclerosis. Brain. 2007; 130(Pt 8):2220–2231. [PubMed: 17664178]
14. Yiannakas MC, Kearney H, Samson RS, et al. Feasibility of grey matter and white matter segmentation of the upper cervical cord in vivo: a pilot study with application to magnetisation transfer measurements. NeuroImage. 2012; 63(3):1054–1059. [PubMed: 22850571]
15. Agosta F, Pagani E, Caputo D, Filippi M. Associations between cervical cord gray matter damage and disability in patients with multiple sclerosis. Arch Neurol. 2007; 64(9):1302–1305. [PubMed: 17846269]
16. Kearney H, Yiannakas MC, Samson RS, Wheeler-Kingshott CA, Ciccarelli O, Miller DH. Investigation of magnetization transfer ratio-derived pial and subpial abnormalities in the multiple sclerosis spinal cord. Brain. 2014; 137(Pt 9):2456–2468. [PubMed: 24966048]
17. Stroman PW, Wheeler-Kingshott C, Bacon M, et al. The current state-of-the-art of spinal cord imaging: Methods. NeuroImage. 2014; 84:1070–1081. [PubMed: 23685159]
18. Kameyama T, Hashizume Y, Ando T, Takahashi A. Morphometry of the normal cadaveric cervical spinal cord. Spine. 1994; 19(18):2077–2081. [PubMed: 7825049]
19. Kretschmann HJ, Tafesse U, Herrmann A. Different volume changes of cerebral cortex and white matter during histological preparation. Microsc Acta. 1982; 86(1):13–24. [PubMed: 7048029]
20. Dietrich O, Reiser MF, Schoenberg SO. Artifacts in 3-T MRI: physical background and reduction strategies. Eur J Radiol. 2008; 65(1):29–35. [PubMed: 18162353]
21. Klein JP, Arora A, Neema M, et al. A 3T MR imaging investigation of the topography of whole spinal cord atrophy in multiple sclerosis. AJNR Am J Neuroradiol. 2011; 32(6):1138–1142. [PubMed: 21527570]
22. Ulbrich EJ, Schraner C, Boesch C, et al. Normative MR cervical spinal canal dimensions. Radiology. 2014; 271(1):172–182. [PubMed: 24475792]
23. Kato F, Yukawa Y, Suda K, Yamagata M, Ueta T. Normal morphology, age-related changes and abnormal findings of the cervical spine. Part II: Magnetic resonance imaging of over 1,200 asymptomatic subjects. Eur Spine J. 2012; 21(8):1499–1507. [PubMed: 22302162]
24. Sigmund EE, Suero GA, Hu C, et al. High-resolution human cervical spinal cord imaging at 7 T. NMR Biomed. 2012; 25(7):891–899. [PubMed: 22183956]
25. Taso M, Le Troter A, Sdika M, et al. Construction of an in vivo human spinal cord atlas based on high-resolution MR images at cervical and thoracic levels: preliminary results. MAGMA. 2014; 27(3):257–267. [PubMed: 24052240]

26. Callot, V., Duhamel, G., Vignaud, A., Cozzone, PJ. Toward a better description of the gray matter spinal cord by using highly resolved diffusion-weighted and morphologic T2*-weighted MRI. Proceeding of the 17th Annual Meeting of ISMRM; Honolulu, HI, USA. 2009. (abstrct 1302)
27. Fonov VS, Le Troter A, Taso M, et al. Framework for integrated MRI average of the spinal cord white and gray matter: The MNI-Poly-AMU template. NeuroImage. 2014; 102(P2):817–827. [PubMed: 25204864]
28. Fradet L, Arnoux PJ, Ranjeva JP, Petit Y, Callot V. Morphometrics of the entire human spinal cord and spinal canal measured from in vivo high-resolution anatomical magnetic resonance imaging. Spine. 2014; 39(4):E262–269. [PubMed: 24253776]
29. Bernstein MA, Thomasson DM, Perman WH. Improved detectability in low signal-to-noise ratio magnetic resonance images by means of a phase-corrected real reconstruction. Med Phys. 1989; 16(5):813–817. [PubMed: 2811764]
30. Moran PR, Kumar NG, Karstaedt N, Jackels SC. Tissue contrast enhancement: image reconstruction algorithm and selection of TI in inversion recovery MRI. Magn Reson Imaging. 1986; 4(3):229–235. [PubMed: 3669934]
31. Park HW, Cho MH, Cho ZH. Real-value representation in inversion-recovery NMR imaging by use of a phase-correction method. Magn Reson Med. 1986; 3(1):15–23. [PubMed: 3959881]
32. Kellman P, Arai AE, McVeigh ER, Aletras AH. Phase-sensitive inversion recovery for detecting myocardial infarction using gadolinium-delayed hyperenhancement. Magn Reson Med. 2002; 47(2):372–383. [PubMed: 11810682]
33. Xiang QS. Inversion recovery image reconstruction with multiseed region-growing spin reversal. J Magn Resonance Imaging. 1996; 6(5):775–782.
34. Borrello JA, Chenevert TL, Aisen AM. Regional phase correction of inversion-recovery MR images. Magn Resonance Med. 1990; 14(1):56–67.
35. Wang J, Chen H, Maki JH, et al. Referenceless Acquisition of Phase-sensitive Inversion-recovery with Decisive reconstruction (RAPID) imaging. Magn Reson Med. 2014; 72(3):806–815. [PubMed: 24407614]
36. Huber AM, Schoenberg SO, Hayes C, et al. Phase-sensitive inversion-recovery MR imaging in the detection of myocardial infarction. Radiology. 2005; 237(3):854–860. [PubMed: 16304107]
37. Hou P, Hasan KM, Sitton CW, Wolinsky JS, Narayana PA. Phase-sensitive T1 inversion recovery imaging: a time-efficient interleaved technique for improved tissue contrast in neuroimaging. AJNR Am J Neuroradiol. 2005; 26(6):1432–1438. [PubMed: 15956512]
38. Christophe C, Muller MF, Baleriaux D, et al. Mapping of normal brain maturation in infants on phase-sensitive inversion--recovery MR images. Neuroradiology. 1990; 32(3):173–178. [PubMed: 2215899]
39. Sanchez-Panchuelo RM, Besle J, Mougin O, et al. Regional structural differences across functionally parcellated Brodmann areas of human primary somatosensory cortex. NeuroImage. 2014; 93(Pt 2):221–230. [PubMed: 23558101]
40. Ishimori T, Nakano S, Mori Y, et al. Preoperative identification of subthalamic nucleus for deep brain stimulation using three-dimensional phase sensitive inversion recovery technique. Magn Reson Med Sciences. 2007; 6(4):225–229.
41. O'Gorman RL, Shmueli K, Ashkan K, et al. Optimal MRI methods for direct stereotactic targeting of the subthalamic nucleus and globus pallidus. Eur Radiol. 2011; 21(1):130–136. [PubMed: 20652256]
42. Nelson F, Poonawalla AH, Hou P, Huang F, Wolinsky JS, Narayana PA. Improved identification of intracortical lesions in multiple sclerosis with phase-sensitive inversion recovery in combination with fast double inversion recovery MR imaging. AJNR Am J Neuroradiol. 2007; 28(9):1645–1649. [PubMed: 17885241]
43. Poonawalla AH, Hasan KM, Gupta RK, et al. Diffusion-tensor MR imaging of cortical lesions in multiple sclerosis: initial findings. Radiology. 2008; 246(3):880–886. [PubMed: 18195384]
44. Sethi V, Yousry TA, Muhlert N, et al. Improved detection of cortical MS lesions with phase-sensitive inversion recovery MRI. Journal Neurol Neurosurg Psychiatry. 2012; 83(9):877–882.

45. Kearney H, Miszkiel KA, Yiannakas MC, Ciccarelli O, Miller DH. A pilot MRI study of white and grey matter involvement by multiple sclerosis spinal cord lesions. Multiple Sclerosis and Related Disorders. 2013; 2:103–108. [PubMed: 25877631]

46. Kearney H, Yiannakas MC, Abdel-Aziz K, et al. Improved MRI quantification of spinal cord atrophy in multiple sclerosis. J Magn Reson Imaging. 2014; 39(3):617–623. [PubMed: 23633384]

47. Poonawalla AH, Hou P, Nelson FA, Wolinsky JS, Narayana PA. Cervical Spinal Cord Lesions in Multiple Sclerosis: T1-weighted Inversion-Recovery MR Imaging with Phase-Sensitive Reconstruction. Radiology. 2008; 246(1):258–264. [PubMed: 17991786]

48. Losseff NA, Webb SL, O'Riordan JI, et al. Spinal cord atrophy and disability in multiple sclerosis. A new reproducible and sensitive MRI method with potential to monitor disease progression. Brain. 1996; 119(Pt 3):701–708. [PubMed: 8673483]

49. Mann RS, Constantinescu CS, Tench CR. Upper cervical spinal cord cross-sectional area in relapsing remitting multiple sclerosis: application of a new technique for measuring cross-sectional area on magnetic resonance images. J Magn Reson Imaging. 2007; 26(1):61–65. [PubMed: 17659556]

50. Rashid W, Davies GR, Chard DT, et al. Upper cervical cord area in early relapsing-remitting multiple sclerosis: cross-sectional study of factors influencing cord size. J Magn Reson Imaging. 2006; 23(4):473–476. [PubMed: 16521094]

51. Rocca MA, Horsfield MA, Sala S, et al. A multicenter assessment of cervical cord atrophy among MS clinical phenotypes. Neurology. 2011; 76(24):2096–2102. [PubMed: 21670439]

52. Lukas C, Sombekke MH, Bellenberg B, et al. Relevance of spinal cord abnormalities to clinical disability in multiple sclerosis: MR imaging findings in a large cohort of patients. Radiology. 2013; 269(2):542–552. [PubMed: 23737540]

53. Horsfield MA, Sala S, Neema M, et al. Rapid semi-automatic segmentation of the spinal cord from magnetic resonance images: application in multiple sclerosis. NeuroImage. 2010; 50(2):446–455. [PubMed: 20060481]

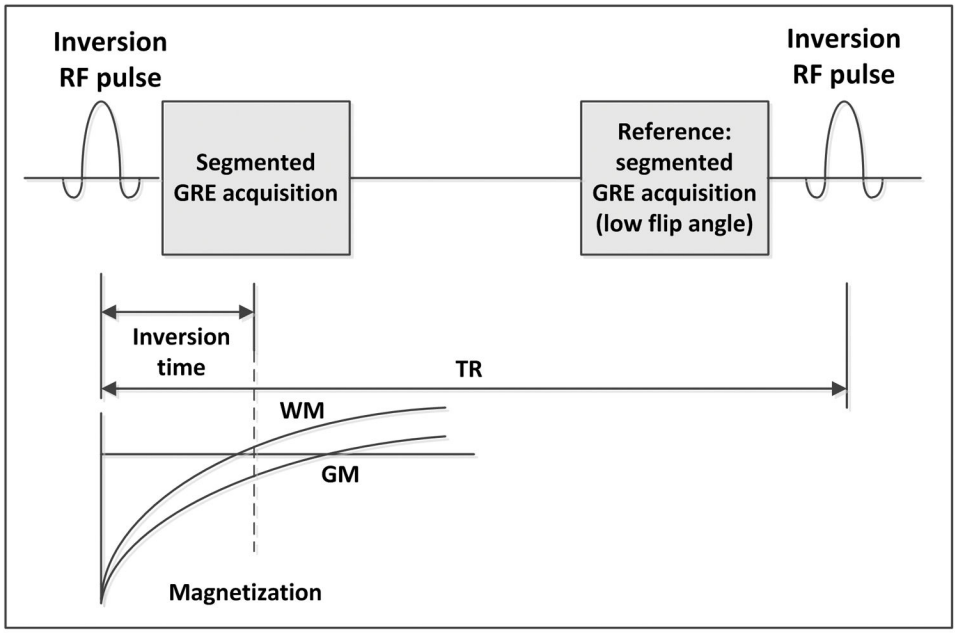

Figure 1.

Pulse sequence diagram of the 2D PSIR acquisition: a non-selective inversion radio frequency (RF) pulse is applied and after an inversion time (TI) a segment of a 2D gradient echo image (GRE) is acquired. The same segment, used as reference for the phase sensitive reconstruction, is reacquired with a low flip angle just before the application of a subsequent inversion RF pulse and the acquisition of the following segment. The time between RF inversion pulses is called repetition time (TR). The magnetization in most of the tissues can be considered almost fully recovered when the reference image is acquired.

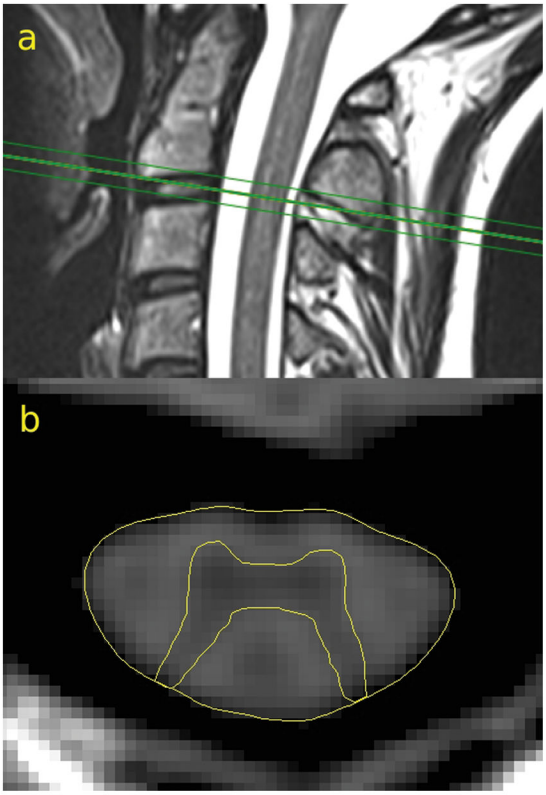

Figure 2.
Positioning of the 2D PSIR acquisition on a sagittal T2 weighted image at the C2–C3 disc level (a). TCA and GM segmentation on the phase-sensitive reconstructed image (b) of a representative subject.

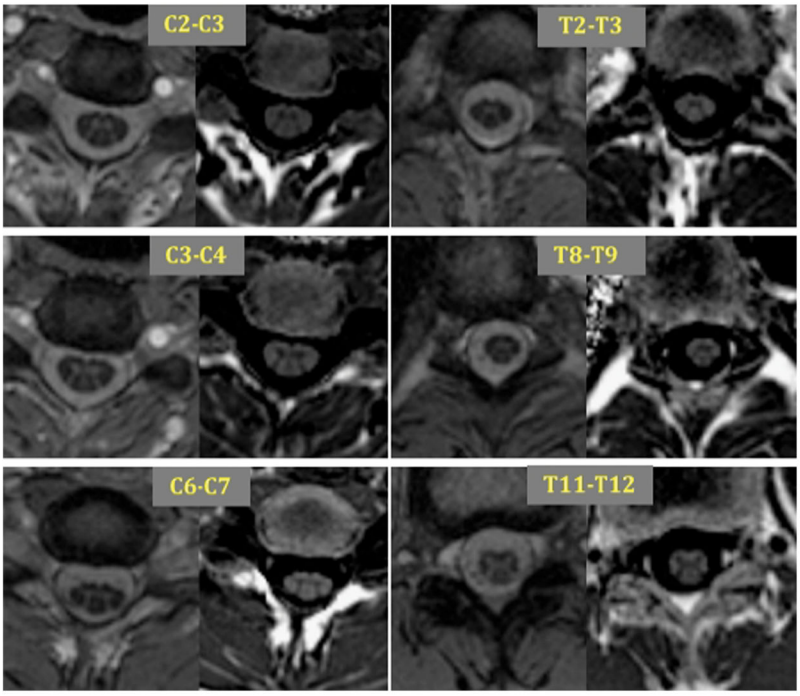

Figure 3.
Six illustrative magnitude (left) and phase-sensitive reconstructed images (right) of spinal cord levels acquired on a healthy control.

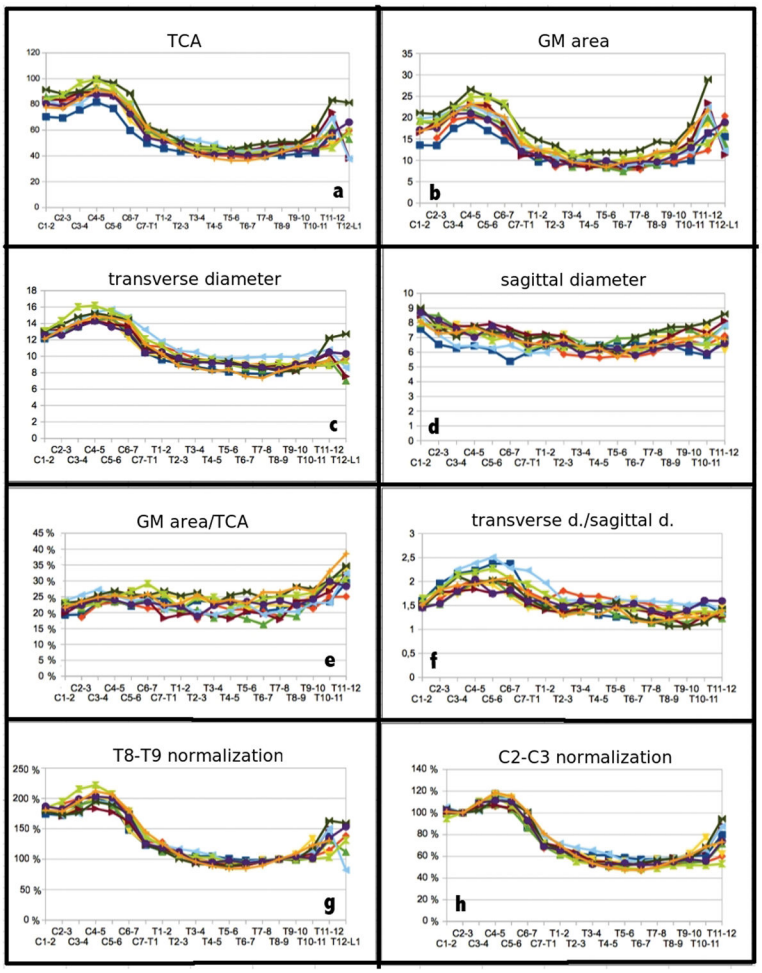

Figure 4.

Entire spinal cord axis morphometric results for 10 healthy controls: a) total cross-sectional area (TCA), b) gray matter (GM) area, c) transverse diameter, d) sagittal diameter, e) GM area/TCA, f) ratio between diameters, g) each level TCA normalized to T8–T9 TCA and h) to C2–C3 TCA. Areas are reported in mm^2 and diameters in mm.

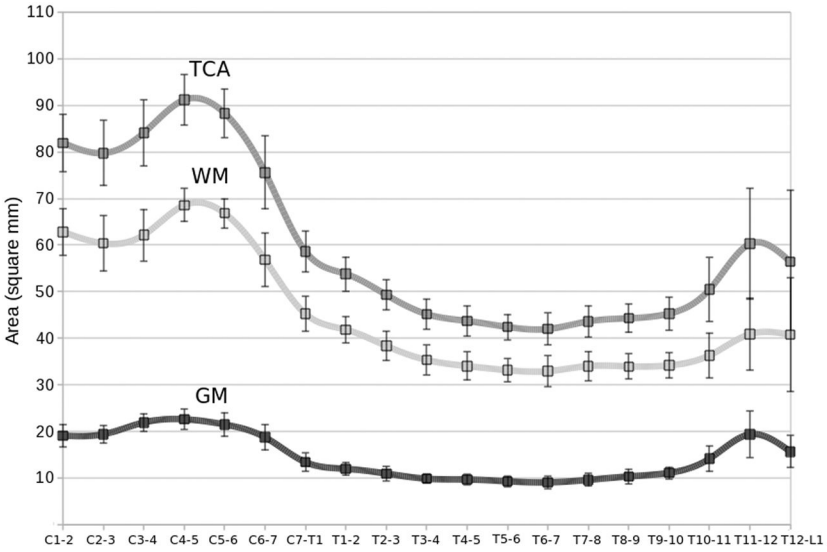

Figure 5.

Group average and standard deviation of the total cross-sectional area (TCA), and the white matter (WM) and gray matter (GM) areas for each level. Data reported are based on 32 subjects at the C2–C3, C3–C4, T8–T9 and T9–T10 disc levels and on 10 subjects at all other levels. Areas are reported in mm^2.

Table 1

Experiment A) Intra-operator scan-rescan reproducibility

	TCA		GM	
	C2–C3	**C3–C4**	**C2–C3**	**C3–C4**
Operator 1	0.4%	1.86%		
Operator 2	0.51%	1.85%	2.17%	2.40%
Operator 3	0.32%	2.62%	3.33%	2.71%
Mean	0.41%	2.11%	2.75%	2.55%

Scan-rescan intra-operator reproducibility coefficient of variation (COV) for the total cross-sectional area (TCA) and gray matter area (GM) measurements in the 4 times repeated acquisition at the C2–C3 and C3–C4 levels.

Table 2

Experiment B) Inter-operator reliability

	TCA				GM			
	C2–C3	**C3–C4**	**T8–T9**	**T9–T10**	**C2–C3**	**C3–C4**	**T8–T9**	**T9–T10**
COV	0.35%	0.25%	0.43%	0.71%	3.18%	3.99%	5.90%	3.72%
ICC	0.999	0.998	0.996	0.998	0.916	0.888	0.912	0.906

Inter-operator reliability coefficient of variation (COV) and intra-class correlation coefficient (ICC) for the total cross-sectional area (TCA) and gray matter area (GM) measurements on 8 subjects at the C2–C3, C3–C4, T8–T9 and T9–T10 levels.

Table 3

Average morphometric results

Cord level	Area (mm^2) TCA	GM	GM/TCA (%)	Diameter (mm) Transverse	Sagittal	TCA/C2–C3 (%)
C1-2	81,9 ± 6,1	19,1 ± 2,4	22,9 ± 2,7	12,7 ± 0,4	8,4 ± 0,5	100,9 ± 3,2
C2-3	79,7 ± 7,0	19,4 ± 1,9	23,8 ± 2,4	13,0 ± 0,8	7,8 ± 0,7	100,0 ± 0,0
C3-4	84.1 ± 7,1	21,9 ± 1,9	25,4 ± 1,6	13,9 ± 0,9	7,5 ± 0,8	105,4 ± 4,4
C4-5	91,2 ± 5,4	22,6 ± 2,1	24,8 ± 1,1	14,8 ± 0,6	7,2 ± 0,5	112,6 ± 4,6
C5-6	88,3 ± 5,2	21,5 ± 2,6	24,3 ± 1,8	14,6 ± 0,6	7,1 ± 0,6	109,0 ± 4,3
C6-7	75,6 ± 7,9	18,7 ± 2,8	24,7 ± 2,0	13,6 ± 0,9	7,0 ± 0,6	93,1 ± 6,2
C7-T1	58,6 ± 4,4	13,4 ± 1,9	22,8 ± 2,7	11,3 ± 0,9	6,6 ± 0,5	72,4 ± 4,2
T1-2	53,8 ± 3,6	12,0 ± 1,4	22,2 ± 1,8	10,5 ± 0,7	6,7 ± 0,4	66,4 ± 3,2
T2-3	49,3 ± 3,2	11,0 ± 1,5	22,2 ± 3,1	9,7 ± 0,6	6,7 ± 0,4	60,9 ± 3,8
T3-4	45,2 ± 3,2	9,8 ± 0,9	21,9 ± 2,1	9,4 ± 0,5	6,3 ± 0,3	55,8 ± 4,3
T4-5	43,7 ± 3,3	9,7 ± 1,1	22,2 ± 2,3	9,3 ± 0,5	6,2 ± 0,3	54,0 ± 4,4
T5-6	42,4 ± 2,7	9,3 ± 1,1	21,9 ± 2,3	9,0 ± 0,5	6,1 ± 0,4	52,4 ± 3,6
T6-7	42,0 ± 3,4	9,1 ± 1,3	21,6 ± 3,0	8,7 ± 0,6	6,3 ± 0,5	51,8 ± 3,4
T7-8	43,6 ± 3,4	9,6 ± 1,4	22,0 ± 2,9	8,6 ± 0,7	6,6 ± 0,5	53,9 ± 3,4
T8-9	44,3 ± 3,1	10,3 ± 1,6	23,3 ± 3,0	8,6 ± 0,4	6,9 ± 0,5	55,6 ± 3,1
T9-10	45,3 ± 3,5	11,1 ± 1,3	24,5 ± 2,0	8,7 ± 0,5	6,9 ± 0,5	56,8 ± 3,8
T10-11	50,4 ± 6,8	14,1 ± 2,8	27,9 ± 3,3	9,2 ± 0,5	6,9 ± 0,7	62,3 ± 8,2
T11-12	60,3 ± 11,9	19,4 ± 4,9	31,6 ± 3,7	9,9 ± 1,1	7,3 ± 0,8	72,4 ± 13,4
T12-L1	56,4 ± 15,4	15,7 ± 3,4	30,9 ± 2,3	9,3 ± 1,9	6,7 ± 1,1	67,3 ± 17,5

TCA: total cross-sectional area; GM: gray matter area; TCA/C2–C3: total cross-sectional area normalized to the C2–C3 level. Levels acquired for all 32 subjects are shown in gray while other lines refer only to the 10 subjects whose entire spinal cord axis was explored.

Table 4

Associations of total cross-sectional and gray matter areas values at the 4 different levels

		C2–C3		C3–C4		T8–T9		T9–T10	
		TCA	**GM**	**TCA**	**GM**	**TCA**	**GM**	**TCA**	**GM**
C2–C3	TCA	**1**	**0.65 (<0.001)**	**0.89 (<0.001)**	**0.76 (<0.001)**	**0.74 (<0.001)**	**0.55 (0.002)**	**0.65 (<0.001)**	**0.63 (<0.001)**
	GM		**1**	**0.51 (0.003)**	**0.58 (0.001)**	**0.68 (<0.001)**	**0.38 (0.041)**	**0.59 (0.001)**	**0.52 (0.004)**
C3–C4	TCA			**1**	**0.85 (<0.001)**	**0.63 (<0.001)**	**0.55 (0.002)**	**0.57 (0.001)**	**0.62 (<0.001)**
	GM				**1**	**0.62 (<0.001)**	0.30 (0.104)	**0.54 (0.002)**	**0.57 (0.001)**
T8–T9	TCA					**1**	**0.49 (0.006)**	**0.89 (<0.001)**	**0.76 (<0.001)**
	GM						**1**	**0.49 (0.006)**	**0.63 (<0.001)**
T9–T10	TCA							**1**	**0.74 (<0.001)**
	GM								**1**

Pearson coefficients and respective p values (reported in brackets) for the relationships of total cross-sectional area (TCA) and gray matter (GM) area in the cohort of 32 subjects at the C2–C3, C3–C4, T8–T9 and T9–T10 disc levels. Statistically significant values are reported in bold.